Anal. Bioanal. Electrochem., Vol. 17, No. 2, 2025, 135-147
https://www.doi.org/10.22034/abec.2025.721566

Analytical & Bioanalytical Electrochemistry

Full Paper

Electrochemical Investigation and Simultaneous Resolution of Uric Acid in the Presence of Guanine at Bismuth Ferrite MWCNT Nanocomposites Modified CPE: A Voltammetric Analysis

Rohini B. Anagawadi, and K.R. Mahanthesha*

Department of Studies in Chemistry, Shivagangothri, Davangere University, Davangere, Karnataka, India

*Corresponding Author, Tel.: +91-9632188239
E-Mail: krmahanthesha@gmail.com

Received: 15 December 2024 / Received in revised form: 23 February 2025 / Accepted: 24 February 2025 / Published online: 28 February 2024

Abstract- An electrochemical sensor for the sensitive and selective measurement of Uric acid in the presence of Guanine is created using bismuth ferrite Multiwalled carbon nanotube (MWCNT) nanocomposites modified carbon paste electrode (MCPE). The simple combustion approach was used to synthesize the bismuth ferrite MWCNT nanocomposites. Bismuth ferrite MWCNT nanocomposite structural morphology and characterization were investigated through the use of EDX, FT-IR, SEM, and powder XRD. At very low concentrations, bismuth ferrite MWCNT nanocomposites had an amazing synergistic effect on Uric acid (UA) electrochemical sensing. Under ideal circumstances, the bismuth ferrite MWCNT nanocomposites MCPE demonstrated good linear properties for the quantitative analysis of UA and GU with a limit of detection 1.56 µM and 0.085 µM respectively, and simultaneous study of UA and GU is carried out by cyclic voltammetry and differential pulse voltammetry. The bismuth ferrite MWCNT nanocomposites MCPE was used for analysis of UA and GU in the real samples.

Keywords- Uric acid; Guanine; Sensors; Sensitive; Combustion Limit of detection; Limit of quantification

1. INTRODUCTION

UA (Uric acid) and GU (Guanine) are two of the main purine bases that form up nucleic acids. They are essential to many aspects of life, including the release of neurotransmitters, blood circulation, and heart rhythm maintenance [1]. The main byproduct of the purine metabolism is UA. The human body typically excretes 1.4–4.4 mM of it in urine and 0.3–0.5 mM of it in serum [2,3] The metabolism of purines like GU results in the formation of UA in the blood [4]. Determining the concentration of UA is crucial since it can lead to disorders like gout, hyperuricaemia, and Lesch-Nyan disease, which are more harmful to tissues than xanthine or hypoxanthine [5]. Therefore, UA needs to be regularly monitored and sensed using a technology that is easy to use, quick, and appropriate. Among these, the UA biosensor has drawn increasing interest due to its benefits of easy production, minimal cost, high sensitivity, and good selectivity [6-8].

GU is important for the regulatory systems that support the preservation of internal settings in living things and tissues. Unusual variations in the concentration and structure of GU in deoxyribonucleic acid (DNA) might result in immune system disturbances, which can manifest as symptoms of various illnesses such as mental retardation, cancer, HIV infection [9]. The main nucleotides in DNA are GU.

Multiferroic materials have great potential for applications in nanoelectronics, spintronics, and sensing because of their simultaneous ferroelectric and ferromagnetic ordering, which has drawn plenty of attention in recent years. Since bismuth ferrite, or $BiFeO_3$, has high Curie and Neel temperatures, it is one of the multiferroic compounds that has been investigated the most [10]. Electrochemical techniques have demonstrated significant popularity in the identification of certain biomolecules [11-18]. Electrochemical sensors make considerable use of electrodes based on carbon. Its effectiveness has been restricted so far, Furthermore, careful surface modification of the carbon-based electrodes using redox mediators has resulted in increased selectivity [19,20]. The combustion pathway is one of the many wet chemical processes that is found to be adaptable, straightforward, and quick, enabling the efficient synthesis of a wide range of nanosized materials [21]. This process depends on taking advantage of the combustion reaction enthalpy, which occurs when a mixture of different organic fuels and the required metal nitrates is heated quickly. The combustion process is self-propagating because of the reaction's strong exothermic nature. Without the need for further annealing, the temperature reached within the reactant system is sufficient to encourage the production of the target chemical [22]. It has been discovered that carbon nanotubes (CNTs) are robust in ambient environments and display a high ambipolar electric field, making them perfect for the construction of electrochemical sensors [23]. The cylindrical nanostructures known as carbon nanotubes (CNTs) are created by rolling hexagonal graphene nets into tubes with nanometer-sized diameters. It is possible to roll graphene in one or more layers. The latter are referred to as multiwalled CNTs (MWCNTs), and the former as single-walled CNTs (SWCNTs) [24].

In this present work, $BiFeO_3$ nanoparticles were synthesized by a simple combustion method, it was mixed with MWCNTs and it was characterized. Hence bismuth ferrite multiwalled carbon nanotubes nanocomposite were used as a modifier for electrochemical sensing. In addition, the peak potential difference for UA-GU was sufficient to detect selectively and individually.

2. EXPERIMENTAL SECTION

2.1. Chemicals and reagents

MWCNT, GU, and UA were purchased from Sigma Aldrich Chemical Company. A solution of 2.5 mM GU and 2.5 mM UA and a supporting electrolyte of 0.2M Phosphate Buffer Solution (PBS) was used. All the chemicals used were AR grade 99%, and the solution was freshly prepared in Double Distilled water.

2.2. Apparatus

Every consideration was used for room temperature. Rigaku Smart Lab A crystal size analysis was conducted using an X-ray diffractometer (XRD). FT-IR alpha spectrophotometer using the KBr pellet technique. The FESEM-CARLZEISS Ultra 55 scanning electron microscope was used to analyze the surface morphology. The CHI-660E potentiostat analytical system model (Electrochemical workstation, USA) was used to perform cyclic voltammetry (CV). A typical electrochemical cell was used for all of the tests. The traditional three-electrode electrochemical cell uses bare carbon paste or bismuth ferrite MWCNT as the working electrode, saturated calomel electrode (SCE) serves as the reference electrode, while platinum wire serves as the counter electrode.

2.3. Synthesis of Bismuth ferrite oxide nanoparticles

When compared to the conventional high-temperature reaction, the combustion approach is undoubtedly the most affordable, energy-efficient, and straightforward way to create Bismuth ferrite oxide nanoparticles. Analytical grade of Bismuth nitrate, Ferric nitrate and fuel as a D-glucose which is dissolved in deionized water and transferred to the silica crucible and kept it in a preheated muffle furnace for about 10min and later on it was calcinated for 3 hours to remove the impurities [25].

2.4. Preparation of CPE and bismuth ferrite MWCNT modified CPE

Silicon oil with fine graphite powder together were combined in 70%:30% ratio and blended by hand for almost half an hour in an agate mortar. The final paste had a 3 mm diameter and was packed in a CPE. Tissue paper was used to smooth the packed carbon paste's surface. By grinding bismuth ferrite multiwalled carbon nanotube nanocomposites in milligrammes

contains 30 percent silicone oil and 70 percent graphite powder, the bismuth ferric MWCNT modified CPE was made.

3. RESULTS AND DISCUSSION

3.1. X-ray diffraction (XRD)

The powder diffraction data can be used to index the XRD patterns of JCPDS Card No. 01-072-2321 this indicates, Bismuth Ferrite MWCNT nanocomposites. Furthermore, the XRD pattern points to the generation of a rhombohedral perovskite structure with extremely crystalline BiFeO3 (R3m space group). Debye Scherrer's formula $D = 0.9\ \lambda /(\beta \cos\theta B)$ (1) was utilized to estimate the average particle sizes of the powders. Here, λ = 1.1541 Ao (X-ray wavelength), D stands for average grain size, and β is the breadth of the diffraction peak at half maximum for the diffraction angle 2θ. According to Debye-Scherrer's formula, the average particle size of Bismuth Ferrite MWCNT nanocomposites is 287 nm [26].

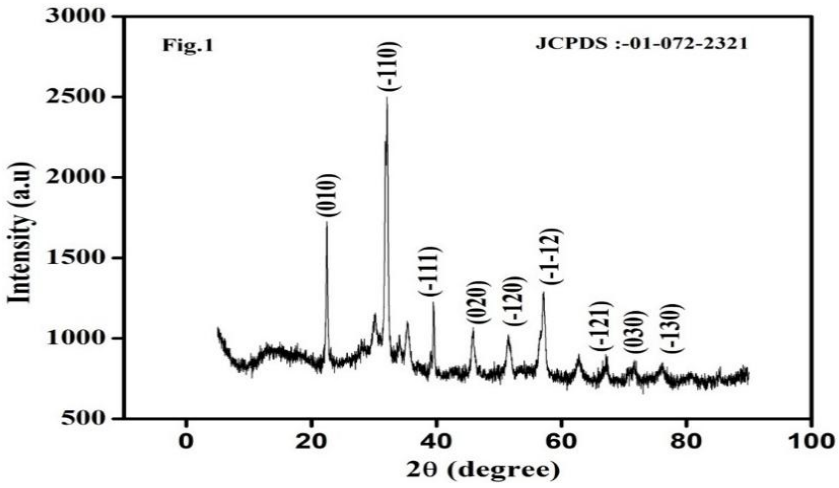

Figure 1. XRD pattern of bismuth ferrite MWCNT nanocomposites

3.2. FT-IR Spectroscopy

To determine the functional groups, present in the produced materials, FTIR analysis was done. Figure 2 shows the FTIR spectra for the synthesized sample, which were recorded in the 500–4000 cm^{-1} region. The stretching vibration modes of Fe-O bonds, which are characteristic of octahedral FeO_6 groups in perovskite compounds, are the cause of the peak located at 547.8 cm^{-1} [27]. Band locations about 1000 cm^{-1}, which correspond to the Bi-O bond's vibration modes, and bands seen between 800 and 1000 cm^{-1}, which correspond to conventional metal-oxygen bonds, provide additional evidence for the development of a highly crystalline phase [28].

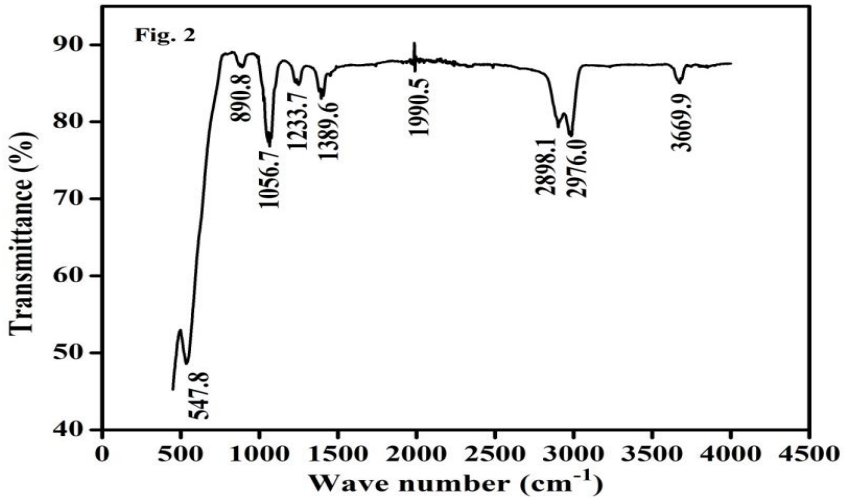

Figure 2. FTIR pattern of Bismuth ferrite MWCNT nanocomposite

3.3. SEM and EDAX Studies

The morphology of the $BiFeO_3$ fig. 3a and $BiFeO_3$ MWCNT nanocomposites Figure 3b is analyzed using FESEM. The $BiFeO_3$ particles formed pendant-like structures and for $BiFeO_3$ MWCNT particles formed pendent over that tubelike structure and both were embedded into the polymeric matrix [29].

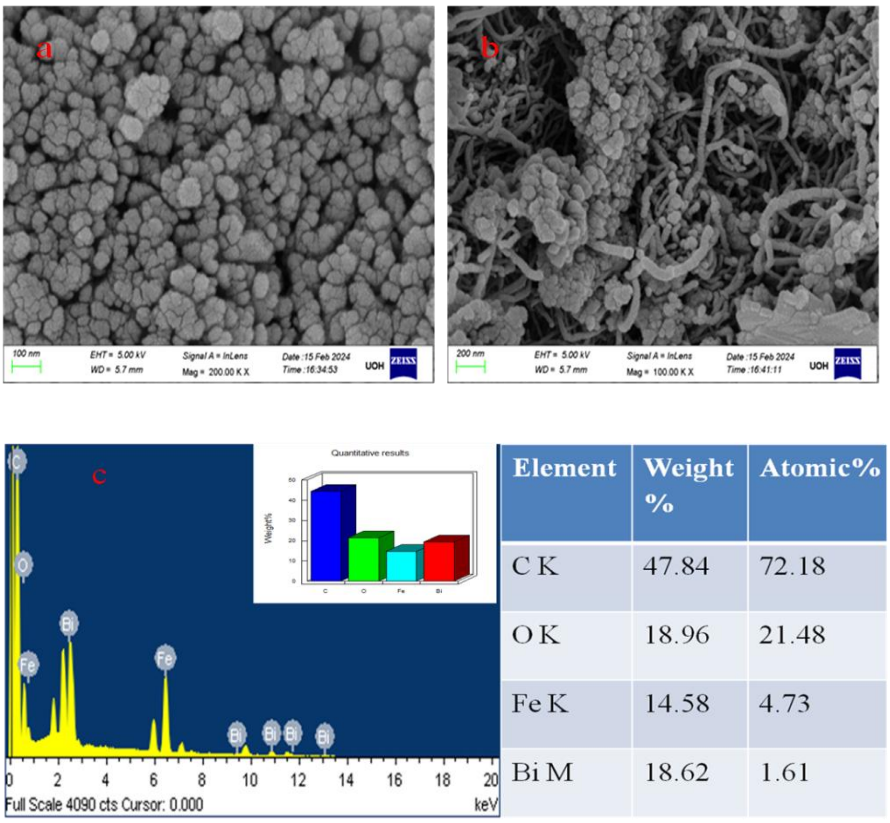

Element	Weight %	Atomic%
C K	47.84	72.18
O K	18.96	21.48
Fe K	14.58	4.73
Bi M	18.62	1.61

Figure 3. (a) SEM image of Bismuth ferrite nanoparticles, (b) SEM image of Bismuth ferrite; MWCNT nanocomposites, (c) EDAX of Bismuth ferrite MWCNT nanocomposites

Investigation indicates that $BiFeO_3$ MWCNTs are evenly dispersed throughout the polymer matrix determines how the composites are polarized [30]. The EDAX detail given in Figure 3c, which shows the EDAX spectrum derived for Bismuth ferrite MWCNT nanocomposites shows the presence of C, O, Fe, and Bi (inset Figure 3c).

3.4. Electrochemical Studies

3.4.1. Active surface area of BCPE and MCPE for Bismuth ferrite MWCNT nanocomposites

In an electrochemical cell, As a supporting electrolyte, a solution of 25 mM $K_4[Fe(CN)_6]$ in 1 M KCl was added. The cyclic voltammograms with scan rates of 0.05 Vs^{-1} are displayed in Fig.4 for the 25 mM $K_4[Fe(CN)_6]$ at BCPE (dotted line-a), Bismuth ferrite MWCNT nanocomposites MCPE (dashed line without analyte-b), and Bismuth ferrite MWCNT nanocomposites MCPE (solid line-c). The prolonged electron transfer phenomena led to a low response in redox peak currents at BCPE. However, with an increase in electron transfer kinetics, the Bismuth ferrite MWCNT nanocomposites MCPE showed a static rise of redox peak currents under the same conditions. The outcome indicates that the modified electrode's surfaces have undergone significant modification, considering the electrocatalytic activity of Bismuth ferrite MWCNT nanocomposites MCPE.

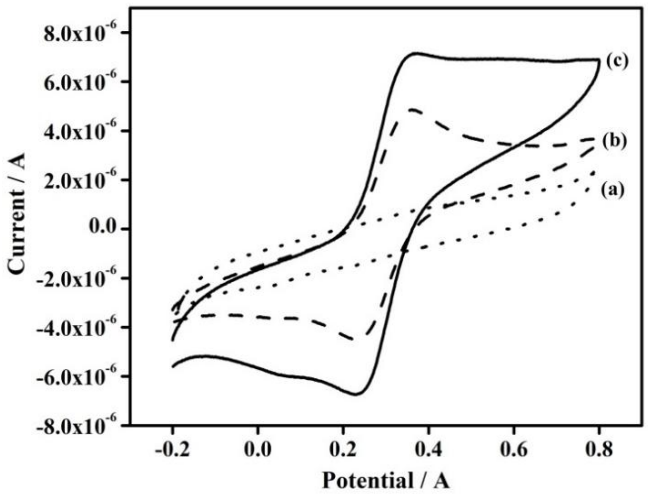

Figure 4. (a) Cyclic Voltammograms of 25 mM $K_4[Fe(CN)_6]$ in 1M KCL solution at BCPE (dotted line); (b) Bismuth ferrite MWCNT nanocomposites MCPE (dash line) in the absence of $K_4[Fe(CN)_6]$; (c) Bismuth ferrite MWCNT nanocomposites MCPE (solid line) in the presence of $K_4[Fe(CN)_6]$

The active surface area of Bismuth ferrite MWCNT nanocomposites MCPE and BCPE is calculated by using Randles- Sevick's equation Eq. (1) [31]:

$$I_p = 2.69\times10^5\, n^{3/2} A\, D^{1/2}\, C_0$$

$$A = I_p / 2.69\times10^5\, n^{3/2}\, D^{1/2}\, C_0 \qquad (1)$$

where I_p stands for peak current, C_0 for analyte concentration, n for electron transfer count, D for diffusion coefficient, Vs^{-1} for scan rate, and A for electroactive surface area (cm^2). Bismuth ferrite MWCNTs nanocomposites. The electroactive surface area of MCPE is 0.0346 cm^2 as compared with BCPE 0.0233 cm^2.

3.4.2. Effect of scan rate on Uric Acid

Voltammograms were taken at different scan rates to investigate the influence of UA at the Bismuth ferrite MWCNT nanocomposites MCPE. Fig. 5a shows the cyclic voltammograms for 2.5 mM UA in 0.2 M PBS at pH 7.0 by varying scan rates at MCPE respectively. The redox peak current increases as the scan rate rises from 50 to 500 mVs^{-1}. In Fig. 5b the graph is plotted against logarithmic anodic peak current (log Ipa) vs. logarithmic scan rate (log υ), Which shows linear connections between log I_{pa} *vs.* log υ. i.e., log I_{pa} = 0.5309 (log υ) -5.1652 with correlation co-efficient (r^2) 0.9940. When the experimental slope approaches the expected value of 0.5 for the optimal electrochemical reaction carried on by the diffusion-controlled process, it will be evident that the behavior of the electrode was, in particular, a diffusion-controlled sensor process [32,33].

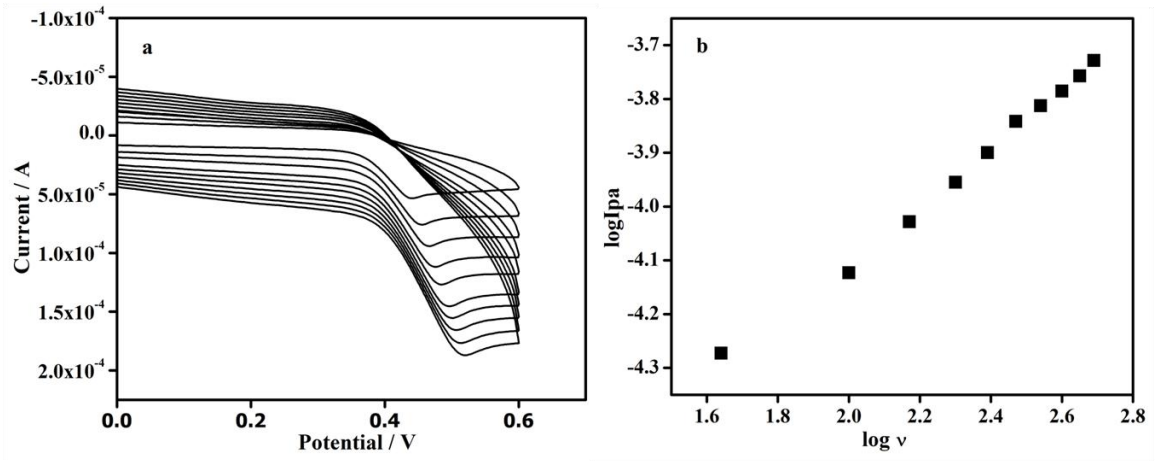

Figure 5. (a) CVs of 25 × 10^{-4} M UA; and (b) log I_{pa} ν/s log υ in assistance with 0.2 M PBS of pH 7.0 with sweep rates 50-500 mVs^{-1} respectively at Bismuth ferrite MWCNT nanocomposites MCPE

3.4.3. Concentration of Uric acid

UA was electrochemically oxidized by altering its concentration at the Bismuth ferrite MWCNT nanocomposites MCPE. Figure 6a demonstrates that when the concentration of UA is increased from 10 to 90 µM, the electrochemical I_{pa} continues to climb with an E_{pa} that tends to the positive, indicating that the product was adsorbed onto the electrode surface.

Additionally plotted the I_{pa} *vs.* UA concentration graph 6b. A correlation coefficient (r^2) of 0.9870 indicates that the graph is linear. This is one way to express the UA anodic peak current: I_{pa} (µA) in linear regression is equal to I_{pa} (µA) = 1.626 (CµM/L) - 5.541×10^{-7}. The detection limit was computed using the formula (2) and quantification limits were calculated by using the formula (3) [34]. The LOD and LOQ were found to be 1.56 µM and 5.2 µM respectively.

$$LOD=3S/M \qquad (2)$$

$$LOQ=10S/M \qquad (3)$$

where S stands for standard deviation and M for slope.

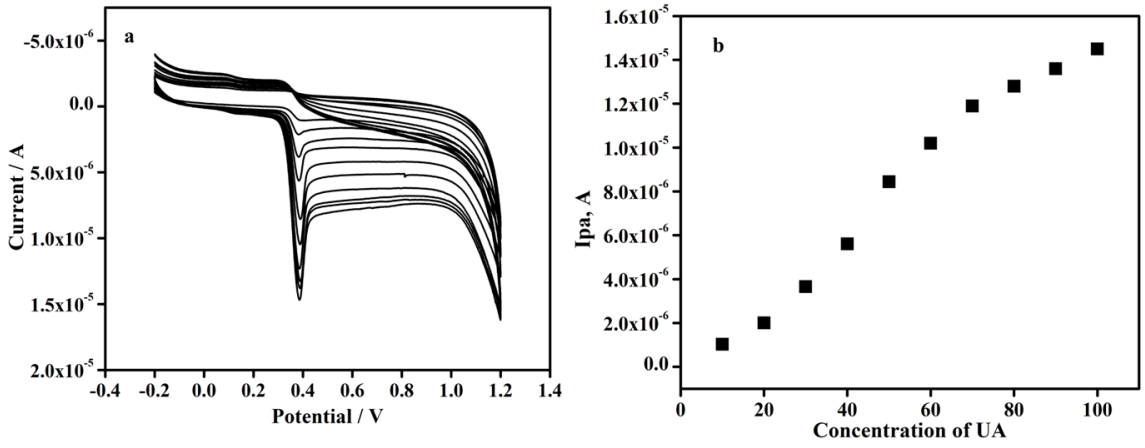

Figure 6. (a) CV for variation of UA concentration from 10 to 90 µM at the MCPE in 0.2 M PBS at pH 7.0. Scan rate 0.05 Vs^{-1}; (b) Graph of the I_{pa} *vs.* concentration of UA

3.4.4. Effect of pH on UA

The electrochemical investigations are significantly impacted by the electrolyte solution's pH, where the reaction is taking place. It has been investigated how pH affects the electro-oxidation of UA (2.5mM) in 0.2 M PBS at varying pH values (5.8–7.8) with a sweep rate of 50 mVs^{-1} at Bismuth ferrite MWCNT nanocomposites MCPE utilizing the CV technique. The CVs for the irreversible oxidation of the UA process are shown in Fig, 7a. As pH levels rise, the peak moves towards negative potential. At Bismuth ferrite MWCNT nanocomposites MCPE, the results yield a linear equation with a slope of 0.057 mV/pH (r^2 = -0.9808) as shown in Figure 7b [35]. All of this suggests that protons and electrons have a major impact on the electrode process during the electrochemical reaction of UA. The correlation's slope indicates that the number of electrons and protons transferred is equal. According to the current work, Bismuth ferrite MWCNT nanocomposites MCPE exhibit strong current augmentation and minimize over potential, and the electrochemical oxidation of UA at this material was a pH-dependent process.

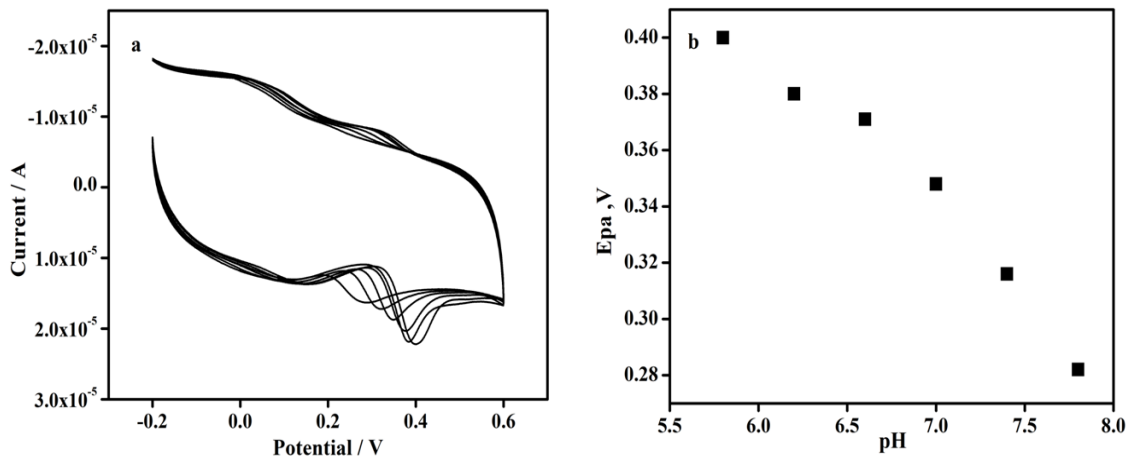

Figure 7. (a) CVs for 10 µM UA at MCPE from pH range 5.8 to 7.8 with scan rate 0.05 Vs^{-1}; (b) Graph of E_{pa} *vs.* pH

3.4.5. Effect of scan rate on GU

Voltammograms were taken at different scan rates to investigate the influence of GU at the Bismuth ferrite MWCNT nanocomposites MCPE. Figure S1 (a) shows the cyclic voltammograms for 2.5 mM GU in 0.2 M PBS at pH 7.0 by varying scan rates at MCPE respectively. The redox peak current increases with an increase in the scan rate from 50 to 400 mVs^{-1}. In S1 (b) the graph plotted against log I_{pa} *vs.* log υ, which shows linear connections between log I_{pa} *vs.* log υ. i.e., log I_{pa} = 0.54 (log υ) - 5.38 with correlation co-efficient (r^2) 0.9623. When the experimental slope approaches the expected value of 0.5 for the optimal electrochemical reaction carried on by the adsorption-controlled process, it will be evident that the electrode behavior was in particular an adsorption-controlled sensor process [32,33].

3.4.6. Effect of concentration of GU

GU was electrochemically oxidized by altering its concentration at the Bismuth ferrite MWCNT nanocomposites MCPE. Figure S2 (a) demonstrates that when the concentration of GU is increased from 10 to 90 µM, the electrochemical I_{pa} continues to climb with an Epa that tends to the positive, indicating that the product was adsorbed onto the electrode surface. Additionally plotted the I_{pa} *vs.* GU concentration, Figure S2 (b), a correlation coefficient (r^2) of 0.9952 indicates that the graph is linear. This is one way to express the GU I_{pa} (µA) in linear regression is equal to I_{pa} (µA)= 2.955 (CµM/L)+7.763×10^{-7}. The detection limit was computed using the formula (2) and quantification limits were calculated by using the formula (3) [34]. The LOD and LOQ were found to be 0.085 µM and 0.286 µM respectively.

3.4.7. Effect of pH on GU

The electrochemical investigations are significantly impacted by the electrolyte solution's pH, where the reaction is taking place. It has been investigated how pH affects the electro-oxidation of GU (2.5 mM) in 0.2 M PBS at varying pH (5.8 to 5.8) with a scan rate of 50 mV

s^{-1} at Bismuth ferrite MWCNT nanocomposites MCPE utilizing the CV technique. The CV for the irreversible oxidation of GU process is shown in Figure S3 (a). As pH levels rise, the peak moves towards negative potential. As pH levels rise, the peak moves towards negative potential. At Bismuth ferrite MWCNT nanocomposites MCPE, the results yield a linear equation with 0.1172 mV/pH as the slope (r^2 = -0.9895) as shown in Figure S3 (b) [35]. All of this suggests that protons and electrons have a major impact on the electrode process during the electrochemical reaction of GU. The correlation's slope indicates that the number of electrons and protons transferred is equal. According to the current work, Bismuth ferrite MWCNT nanocomposites MCPE exhibit strong current augmentation with minimization in overpotential, and the electrochemical oxidation of GU at this material was a pH-dependent process.

3.4.8. Simultaneous study of UA and GU in cyclic Voltammetry

With a variable redox peak current, it yields a broad peak for UA and GU at BCPE. However, two distinct peaks for UA and GU are seen in Bismuth ferrite MWCNT nanocomposites MCPE. It was discovered that the difference between the peaks of UA and GU was 0.33 mV as seen in Figure S4.

We also examined the electro-oxidation processes of UA and GU, one analyte's concentration changed, whereas the other analyte's concentration stayed the same. Using the data displayed in Figure S5 (a). UA concentration varied in the dynamic range from 10 to 80 µM, at the constant concentration of GU. The GU concentration varied from 10 to 80 µM, while UA concentration remained constant in Figure S5 (b). Hence, we found that when the analyte concentration rises, the oxidation peak current rises as well respectively.

3.4.9. Simultaneous study of UA and GU in differential pulse Voltammetry (DPV)

Using DPV to record the anodic peak current on the Bismuth ferrite MWCNT nanocomposites MCPE has been used to increase the sensitivity for the simultaneous assessment of UA and GU. While the concentration of one analyte was initially maintained throughout the experiment, the concentration of the other analyte fluctuated. Figure S6 (a) shows that UA concentration was varied and GU concentration was kept constant. In Figure S6 (b) GU concentration was varied and UA concentration was kept constant. The peak current rises quickly as the corresponding analyte concentration rises because of enhanced current sensitivity and a lack of background current [36].

3.4.10. Real sample analysis

Investigation of UA and GU in Urine samples are found by MCPE using proper addition method. All samples were dissolved in 0.2 M PBS pH.7, the above samples were taken in an electrochemical cell. The current was determined by using the cyclic voltammetric technique

and the results are shown in Table 1. This shows it has excellent sensitivity for identifying UA and GU in real samples.

Table 1. Analysis of UA and GU in Real sample

Content	Uric acid			Guanine		
	Added/µM	**Found/ µM**	**Recovery %**	**Added/ µM**	**Found/ µM**	**Recovery %**
Urine sample	10	10.25	102.5	10	10.3	103
	20	20.12	100.6	20	19.91	99.55
	30	30.22	100.7	30	30.11	100.3

4. CONCLUSION

In this study, Bismuth ferrite MWCNT nanocomposites were synthesized by the combustion method. Using the XRD data. Moreover, the crystallinity and particle size were identified. The average particle size was 287nm. Bismuth ferrite MWCNT nanocomposites consist of the pendent over that tubelike structure as seen in the FESEM. By FTIR data metal oxygen bonds and water traces are observed. For electrochemical detection of UA and GU, a highly stable, sensitive, and selective electrode is made using these Bismuth ferrite MWCNT nanocomposites MCPE. To further explore various parameters electrochemically, cyclic and differential pulse voltammetric techniques are employed, and the synthesized nanocomposites were utilized in the creation of Bismuth ferrite MWCNT nanocomposites MCPE. For UA and GU sensing, the Bismuth ferrite MWCNT nanocomposites MCPE showed excellent electrocatalytic activity and low-level detection limits. It was discovered that the Bismuth ferrite MWCNT nanocomposites MCPE were promising materials for electrodes that will be applied to selectively identify UA while GU is present and vice-versa. The Bismuth ferrite MWCNT nanocomposites MCPE can be used to determine UA and GU in Real sample analysis was justifiable.

Declarations of interest

The authors declare no conflict of interest in this reported work.

REFERENCES

[1] A. A. Ensafi, M Jafari-Asl, B. Rezaei, and A.R. Allafchian, Sens. Actuators B 177 (2013) 634.

[2] N. Misra, V. Kumar, L. Bordeb, L. Varshney, Sens. Actuators B 178 (2013) 371.

[3] H. Manjunatha, D.H. Nagaraju, G.S. Suresh, and T.V. Venkatesha, Electroanalysis 21 (2009) 2198.
[4] L.M. Niu, K.Q. Lian, H.M. Shi, Y.B. Wu, W. J. Kang, and S.Y. Bi, Sens. Actuators B, 178, (2013) 10.
[5] V.V.S. E Dutt, and H.A. Mottola, Anal. Chem. 46 (1974) 1777.
[6] H. Dai, N. Wang, D. Wang, X. Zhang, H. Ma, and M. Lin, Microchim. Acta 183 (2016) 3053.
[7] C. Hou, H. Liu, D. Zhang, and M. Zhang, J. Alloys Compd. 666 (2016) 178.
[8] J. Zhao, F. Mu, L. Qin, X. Jia, and C. Yang, Mater. Chem. Phys. 166 (2015) 176.
[9] G. Boopathy, M. Keerthi, S.M. Chen, M.J. Umapathy, M. Govindasamy, T.W. Chen, M.A. Ali, F.M.A. Hemaid, and M.S. Elshikh, J. Electrochem. Soc. 165 (2018) B651.
[10] J.B. Neaton, C. Ederer, U.V. Waghmare, N.A. Spaldin, and K.M. Rabe, Phys. Rev. B 71 (2005) 014113.
[11] M. Jamal, S. Chakrabarty, M.A. Yousuf, A. Khosla, and K.M. Razeeb, Microsyst. Technol. 24, (2018) 4193.
[12] P. Norouzi, V.K. Gupta, F. Faridbod, M.P. Hamedani, B. Larijani, and M.R. Ganjali, Anal. Chem. 83 (2011) 1564.
[13] M. Kumar, B.E.K. Swamy, S. Reddy, J.K.S. Kumara, and W. Zhao, J. Electrochem. Soc.167 (2020) 087511.
[14] R. Ahmad, M. Khan, N. Tripathy, M.I.R. Khan, and A. Khosla, J. Electrochem. Soc. 167 (2020) 107504.
[15] V. Arabali, M. Ebrahimi, M. Abbasghorbani, V.K. Gupta, M. Farsi, M.R. Ganjali, F. Karimi, J. Mol. Liq. 213 (2016) 312.
[16] M. Jamal, S. Chakrabarty, H. Shao, D. McNulty, M.A. Yousuf, H. Furukawa, A. Khosla, and K.M. Razeeb, Microsyst. Technol. 24 (2018) 4217.
[17] H. Vidya, and B.E.K. Swamy, J. Mol. Liq. 211 (2015) 705.
[18] R.N. Goyal, V.K. Gupta, S. Chatterjee, Biosens. Bioelectron. 24 (2009) 1649.
[19] H.K. Maleh, F. Karimi, S. Malekmohammadi, N.Z.R. Esmaeili, S. Rostamnia, M. LütfiYola, N. Atar, S. Movaghgharnezhad, S. Rajendran, A. Razmjou, Y. Orooji, S. Agarwal, V.K. Gupta, J. Mol. Liq. 310 (2020) 113185.
[20] A. Dhanjai, X. Sinha, L. Lu, J.D. Wu, Y. Tan, J. Li, and R. Chen, Trends Anal. Chem. 98 (2018) 174.
[21] S. Aruna, and A.S. Mukasyan, Mater. Sci. 12 (2008) 44.
[22] R. Ianos, I. Lazău, C. Pãcurariu, and P. Barvinschi, Eur. J. Inorg. Chem. 6 (2008) 931.
[23] K.S. Novoselov, A.K. Geim, S.V. Morozov, and D. Jiang, Phys. Rev. Lett. 306 (2004) 666.

[24] G. Zhi, and Z. Gao, Proceedings of the 1st International Conference on Construction on Developing Countries (ICCIDC1 ’08), Advancing and Integrating Construction Education, Research & Practice, Pakistan, Iran (2008).
[25] P. Priyadharsini, A. Pradeep, C. Murugesan, P.M. Md Gazzali, and G. Chandrasekaran1, Combust. Sci. Technol. 186 (2014) 297.
[26] T.M. Bawazeer, M.S. Alsoufi, M. Shkir, B.M. Al-Shehri, and M.S. Hamdy, Inorg. Chem. Commun. 130 (2021) 108668.
[27] C. Chen, J. Cheng, S. Yu, L. Che, Z. Meng, J. Cryst. Growth 291 (2006) 135.
[28] I. Troyanchuk, A. Chobot, O. Mantytskaya, and N. Tereshko, Inorg. Mater. 46 (2010) 424.
[29] S. Moharana, M.K. Mishra, M. Chopkar, and R.N. Mahaling, Polym. Bull. 74 (2017) 3707.
[30] K. Yu, Y. Niu, Y. Bai, Y. Zhou, and H. Wang, Appl. Phys. Lett. 102 (2013) 102903.
[31] X. Li, and J. Zang, J. Phys. Chem. C 113 (2009) 19411.
[32] S.P. Selvam, and K. Yun, Sens. Actuators B Chem. 302 (2020) 127161.
[33] A.A. Rafati, A. Afraz, A. Hajian, and P. Assari, Microchim. Acta 181 (2014) 1999.
[34] H. Devnani, N. Rashid, and P.P. Ingole, Chem. Select 4 (2019) 633.
[35] Y. Zhang, G.G. Jin, Y. Wang, and Z. Yang, Sensor 10 (2003) 443.
[36] D.A. Balram, K.Y. Lian, and N. Sebastian, Int. J. Electrochem. Sci. 13 (2018) 1542.